INSTITUTO DE FÍSICA preprint

IFUSP/P-293

ELECTROFISSION OF ^{234}U, ^{236}U AND ^{238}U: ANGULAR DISTRIBUTIONS AND E2 STRENGTH FUNCTIONS

by

J.D.T.Arruda-Neto, S.B.Herdade, I.C.Nascimento
Instituto de Física, Universidade de São Paulo.

and

B.L.Berman
Instituto de Física, Universidade de São Paulo
and DPh-N/MF, Centre d'Études Nucléaires de Saclay.

SEP/81

UNIVERSIDADE DE SÃO PAULO
INSTITUTO DE FÍSICA
Caixa Postal - 20.516
Cidade Universitária
São Paulo - BRASIL

ELECTROFISSION OF ^{234}U, ^{236}U, AND ^{238}U: ANGULAR DISTRIBUTIONS AND E2 STRENGTH FUNCTIONS*

J.D.T. Arruda-Neto, S.B. Herdade, I.C. Nascimento,
Instituto de Física, Universidade de São Paulo, São Paulo, Brazil,

and

B.L. Berman+,
Instituto de Física, Universidade de São Paulo, São Paulo, Brazil
and DPh-N/MF, Centre d'Études Nucléaires de Saclay,
91191 Gif-sur-Yvette, France

ABSTRACT

The electrofission angular distributions for ^{234}U in the energy range 5.5 to 25 MeV were measured and are analyzed together with those obtained previously for ^{236}U and ^{238}U. The competition between the K=0 and K=1 fission channels following E2 excitation is established, showing a dominance of the K=0 channel for near-barrier fission. The E2 fission strength functions for ^{234}U, ^{236}U, and ^{238}U are deduced as well, and the E2 fission probabilities (at energies below the pairing gap) are estimated. A substantial concentration of E2 strength near the fission barrier is found, in good agreement with earlier photofission angular-distribution studies.

* Supported in part by FAPESP, CNPq and FINEP (Brazilian sponsors).

+ Permanent address: Lawrence Livermore Laboratory, University of California, Livermore, Calif. 94550.

1. INTRODUCTION

The isoscalar giant quadrupole resonance (GQR), extensively studied in the last decade, is the best known of the "new giant resonances", i.e., those with multipolarity other than El. Recently, the main interest has shifted toward the decay properties of the giant multipole resonances, which can be expected to contribute to our understanding of these fundamental modes of nuclear excitation. For the GQR, theoretical calculations indicate that for heavy nuclei the energy stored in this collective mode of excitation is dissipated primarily by thermalization of the energy and subsequent statistical decay[1]. Therefore, one would expect that for the GQR the decay width of the fission channel in actinide nuclei would be similar to that for the compound nucleus.

The first study of the GQR fission decay (for ^{238}U) was performed by means of a simultaneous analysis of electrofission and photofission cross sections[2,3]. Since then, the other long-lived even-mass uranium isotopes have been studied as well[4,5]. In these studies, substantial E2 strength was detected in the fission channel. An estimate of the E2 fission probability $P_f(E2)$ of 40±10% near 9-10 MeV was obtained for ^{238}U, in accordance both with statistical calculations[3] and with preliminary (e,e'f) coincidence measurements[6].

However, recent hadron-induced fission measurements have yielded contradictory results. For example, van der Plicht et al.[7] claimed, from α-induced fission measurements, that the fission decay of the GQR for ^{238}U (and for ^{232}Th as well) is inhibited strongly, while a similar but newer $^{238}U(\alpha,\alpha'f)$ measurement[8] has yielded $P_f(E2) = 0.25 \pm 0.10$ for the K=0 component of the GQR. Finally, the results for ^{6}Li-induced fission[9] are less conclusive, but a clear structure was observed in the fission coincidence spectrum near the peak energy of the GQR. [We refer

the reader to Ref. 10) for a more complete discussion of the discrepancies between the results of hadron-induced nuclear reactions and those for reactions induced by electromagnetic probes.]

In addition to the controversy concerning the total amount of E2 strength concentrated in the fission decay channel for actinide nuclei, another point of conflict concerns the distribution of E2 strength over the excitation-energy region in which the GQR is found. From the electron-induced results we believe that the GQR strength function peaks at energies below 9 MeV (see section 4.1), whereas from the hadron-induced results the GQR peaks systematically at ~11 MeV and vanishes below ~8.5 MeV. Therefore, it is necessary to study carefully the E2 strength distribution close to the fission barrier (<8 MeV) by means of an unambiguous experimental technique, such as the measurement of the electrofission-fragment angular distributions, which can help to delineate the low-lying fission levels populated by E2 photoabsorption. In so doing, we hope to show that the picture drawn from the hadron-induced fission results, namely, zero E2 fission strength at excitation energies $\lesssim$ 8 MeV for actinide nuclei, is physically unreasonable.

A type of data eminently suitable for the study of the low-lying levels in the fission spectrum (at the saddle point) is the angular distribution of fission fragments induced by real (via photofission) and virtual (via electrofission) photons, especially for even-even nuclei. Also, the low-energy electro- and photofission cross sections reflect barrier-penetration effects and, therefore, constitute a sensitive means for the study of the nature of the fission barrier. However, most of the experimental data bearing upon this problem have been obtained via particle-induced fission, wherein the spectra of the transition nuclei are much more complicated than for photofission and the interpretation of the data is thus much more difficult.

Most of the low-energy photofission studies have been carried out using bremsstrahlung produced in electron accelerators because this is the easiest way to obtain an intense photon flux. The principal drawbacks of this experimental method are a) the necessity of unfolding the yield curves obtained with a continuous photon spectrum and b) the difficulty of sampling multipolarities other than E1. The advantage of using electrofission, relative to photofission, results mainly from the fact that the E2 and M1 virtual-photon spectra are much more intense than the E1 spectrum, as has been demonstrated recently[11]. As a consequence, whereas the anisotropy of photofission angular distributions disappears quickly as the excitation energy is increased (to ~2 MeV above the fission barrier), the electrofission anisotropy remains large significantly above the fission barrier[11]. We refer the reader to Refs. 11-14) for more details.

A formalism for the analysis of electrofission-fragment angular distributions, utilizing the virtual-photon spectrum technique, was developed recently[11]. The application of this formalism to ^{238}U led to the identification of the low-lying (J^{π},K) levels of the transition nucleus, including the $(1^+,1)$, $(2^+,1)$, and $(2^+,2)$ levels never seen before in photofission experiments; also, the competition between the K=0 and K=1 channels of the fission decay following E2 excitation in ^{238}U was delineated. In this paper we extend the application of this formalism to the study of ^{234}U and ^{236}U in order to obtain information about the K=0 and K=1 fission channels for E2 excitation at energies close to the fission barrier. Also, we extract the E2 strength functions for $^{234,236,238}U$ at low excitation energies; by comparing them to the angular-distribution data we establish limits for the E2 strength for the K=0 and K=1 fission channels.

The present work also includes a) the interpretation of our recent results of the GQR fission decay for $^{234,236,238}U$ (obtained from electrofission measurements performed at this Laboratory) in terms of strength functions, from which we obtain the corresponding GQR parameters (peak energy, width, and total strength); b) a discussion of the distribution of the GQR strength obtained in a) in comparison with recent calculations of the fragmentation of the GQR in deformed nuclei[15], showing the crucial role played by the low-energy strength (below ~8.5 MeV, and never sampled in hadron-scattering experiments); and c) an estimate of the E2 fission probabilities $P_f(E2)$ from the experimentally determined strength functions in comparison with statistical calculations at energies close to the fission barrier.

2. RELEVANT THEORY

2.1. Photonuclear and photofission cross sections

The cross section for the nuclear absorption of a photon of energy ω leading to an isolated level ω_R (a giant electric resonance EL, for example) is[3,16]

$$\sigma_\gamma(EL,K_i;\omega) = (2\pi)^3\,\alpha\,\frac{(L+1)}{L[(2L+1)!!]^2}\,\omega^{2L-1}\,\frac{dB}{d\omega}(EL,K_i;\omega) \qquad (1)$$

where $K_i = 0,1,2,\ldots,L$ are the components of the resonance EL. If the strength function $dB/d\omega$ is well represented by a Breit-Wigner-shaped curve, that is,

$$\frac{dB}{d\omega}(EL,\omega) = \sum_{K_i}\frac{dB}{d\omega}(EL,K_i;\omega) = \left[\frac{dB}{d\omega}(EL)\right]_{max}\frac{\Gamma_R^2/4}{(\omega-\omega_R)^2+\Gamma_R^2/4} \qquad (2)$$

then the total EL-strength is given by

$$B(EL) = \int\frac{dB}{d\omega}(EL,\omega)\,d\omega = \frac{\pi}{2}\,\Gamma_R\left[\frac{dB}{d\omega}(EL)\right]_{max}. \qquad (3)$$

Whether or not a Breit-Wigner-shaped curve is appropriate, it is still true that the dependence upon energy of the strength function is given by $\frac{dB}{d\omega}(EL,\omega) \propto \omega^{-(2L-1)}\sigma_\gamma(EL,\omega)$, as would be obtained from a total photonuclear cross-section measurement with monoenergetic photons, and the total strength by $B(EL)\propto\int\omega^{-(2L-1)}\times$ $\times\,\sigma_\gamma(EL,\omega)\,d\omega$. We note that for the special case of L=1 (the GDR), $B(E1)\propto\int\omega^{-1}\sigma_\gamma(E1,\omega)\,d\omega$, as would be obtained from an integral measurement with bremsstrahlung photons because the bremsstrahlung spectrum is to a reasonable approximation proportional to ω^{-1}.

Furthermore, any partial photonuclear cross section $\sigma_{\gamma,x}(EL,\omega)$ can be written as the product of the total cross section and the branching ratio for the (γ,x) reaction $\frac{\Gamma_x}{\Gamma}(EL,\omega)$, so that the decay-channel strength function $\frac{dB}{d\omega}(EL,\omega)\Big|_x \propto \omega^{-(2L-1)}\sigma_\gamma(EL,\omega)\times$ $\times\,\frac{\Gamma_x}{\Gamma}(EL,\omega)$. For example, the fission strength function referred to below is simply $\frac{dB}{d\omega}(EL,\omega)\,\frac{\Gamma_f}{\Gamma}(EL,\omega)$.

We consider now the fission decay mode of an even-even nucleus (ground state $J^\pi,K=0^+,0$), where $\frac{\Gamma_f}{\Gamma}(J^\pi,K)$ is the relative fission probability for the nucleus at the transition state (J^π,K); the photofission cross section is $\sigma_{\gamma,f}(EL,K_i,K;\omega)=\sigma_\gamma(EL,K_i;\omega)\times$ $\frac{\Gamma_f}{\Gamma}(J^\pi,K;\omega)$. However, the initial value K_i for an excited state at or near the ground-state deformation (which is equal to the K-component of the giant EL resonance) is not conserved during the evolution of nuclear shapes to the highly deformed saddle-point shape: in going from the original compound nucleus to the saddle point the nucleus can redistribute its energy and angular momentum in many ways[14]. The K-values of the nuclear transition states (J^π,K) are, therefore, unrelated to the initial value K_i of the compound nucleus. However, it is assumed that once the nucleus

reaches the saddle point (wherever it might be), K is a good quantum number [from this point to the configuration of separated fragments (the scission point)]; that is, the K-distribution is "frozen-in" at the saddle point (usually the outer barrier for the uranium isotopes) for low-energy fission. Assuming, in principle, that the values for K_i are indistinguishable in the experimentally determined photofission cross section, we have

$$\sigma_{\gamma,f}(EL,K;\omega) = \left[\sum_{K_i} \sigma_\gamma\ (EL,K_i;\omega)\right] \cdot \frac{\Gamma_f}{\Gamma}\ (J^\pi,K;\omega) \quad . \qquad (4)$$

2.2. Electron-induced reactions

Electron-induced reactions have proven to be a powerful tool for studying nuclear structure; the basic reasons are that the electron-nucleus interaction is well known and that it is weak (compared to the strong nucleon-nucleus interaction). Therefore, we can perform measurements whithout significant perturbation of the structure of the target nucleus, in contrast with hadron-induced reactions where it is difficult to separate the reaction mechanism from target-structure effects.

The differential electron-scattering cross section, for an individual and well-separated level, calculated in first Born approximation (one-photon exchange) is given by[17]

$$\frac{d\sigma}{d\Omega_{e'}}(EL) = 4\pi\sigma_M\ |F^L(q)|^2 = 4\pi\sigma_M \left\{\frac{q_\mu^4}{q^4}\ |F_C^L(q)|^2 + \right.$$

$$\left. + \left[\frac{q_\mu^2}{2q^2} + \tan^2\left(\frac{\theta_{e'}}{2}\right)\right]\ |F_T^L(q)|^2\right\} \qquad (\hbar=c=1) \qquad (5)$$

for electric transitions of multipolarity L. In eq. (5), σ_M is the Mott cross section (for scattering from a point charge), q is the momentum transferred to the nucleus, $q_\mu^2 = q^2 - \omega^2$, $\omega = E_e - E_{e'}$ is the excitation energy, and $|F_C^L(q)|^2$ and $|F_T^L(q)|^2$ are the squared Coulomb and transverse nuclear form factors, respectively, which are related to the reduced transition probabilities by

$$\left.\begin{aligned} B(CL,q) &= \left[(2L+1)!!\right]^2 \cdot \frac{|F_C^L(q)|^2}{q^{2L}} \qquad \text{and} \\ B(EL,q) &= \frac{L}{(L+1)}\ \left[(2L+1)!!\right]^2 \cdot \frac{|F_T^L(q)|^2}{q^{2L}} \quad . \end{aligned}\right\} \qquad (6)$$

Considering nuclear levels J_f possessing intrinsic widths that cause them to overlap, with a Breit-Wigner shape, one obtains from eqn.(5) that[17]

$$\frac{d^2\sigma(EL)}{d\Omega_{e'}d\omega} = 2\sigma_M \sum_{J_f} \left[\frac{\Gamma^{tot}_{J_f}}{(\omega-\omega_{J_f})^2 + (\Gamma^{tot}_{J_f}/2)^2}\right] \cdot |F^L(q)|^2 \quad . \qquad (7)$$

Eqn.(7) assumes that the dependence upon ω of the form factors can be neglected; the normalization is such that $\int \frac{d^2\sigma(EL)}{d\Omega_{e'}d\omega}\, d\omega = \frac{d\sigma(EL)}{d\Omega_{e'}}$; and $\Gamma^{tot}_{J_f}$ is the total width of the level.

The physical quantity which relates the electron excitation process to the nuclear photoabsorption is the strength function $\frac{dB}{d\omega}(EL,q=\omega)$, that is, the reduced transition probability per unit excitation energy interval, evaluated at the photon point $q=\omega$. Combining eqns.(1), (2), (3), and (7), it is straightforward to show that

$$\frac{1}{4\pi\sigma_M}\ \frac{d^2\sigma(EL)}{d\Omega_{e'}d\omega} = \left[\frac{1}{B(EL)}\ \frac{dB}{d\omega}\ (EL,\omega)\right] \cdot |F^L(q)|^2 \quad . \qquad (8)$$

The strength function $dB/d\omega$ at the photon point is related in turn (using the notation of Donnelly and Walecka[18]) to the longitudinal and transverse dynamic structure functions (or nuclear response surfaces) $S_C^L(q,\omega)$ and $S_T^L(q,\omega)$ by

$$\left.\begin{aligned} \frac{S_C^L(q,\omega)}{M_T} &= \frac{1}{B(EL)} \frac{dB(EL,\omega)}{d\omega} \cdot |F_C^L(q)|^2 \quad \text{and} \\ \frac{S_T^L(q,\omega)}{M_T} &= \frac{1}{B(EL)} \frac{dB(EL,\omega)}{d\omega} \cdot |F_T^L(q)|^2 \end{aligned}\right\} \qquad (9)$$

where M_T is the initial target mass. The response surfaces contain all of the information on the distribution of the nuclear electromagnetic current density; we refer the reader to Ref.18) for a detailed discussion of the nuclear structure information contained in these response surfaces.

2.3. Comparison of photon- and electron-induced reactions

It is useful to compare the photo- and electronuclear cross sections in the same language. A (γ, tot) measurement with monoenergetic photons is specific in ω and sums over all the decay channels, and yields the strength function directly; such a measurement with bremsstrahlung integrates over ω (with the real bremsstrahlung spectrum) and yields the total strength. A (γ,x) measurement selects a single decay channel, and thus yields the product of the strength function (for monoenergetic photons) or the strength (for bremsstrahlung) and the branching ratio. An (e,e') measurement is specific in both ω and q, sums over decay channels, and yields the product of the strength function and the normalized form factor. An (inclusive) (e,x) measurement selects a single decay channel and integrates over both ω and q; however, because an inclusive measurement is dominated by events near the photon point, it yields, to a good approximation (with no form-factor dependence), the product of the strength function and the branching ratio. Finally, an (e,e'x) measurement is specific in both ω and q and also selects a single decay channel, so that it yields the product of three factors: the strength function, the form-factor and the branching ratio. Thus an (e,e') measurement is complementary to a (γ, tot) measurement with monoenergetic photons, an (e,x) measurement to a (γ,x) measurement with bremsstrahlung, and an (e,e'x) measurement to a (γ,x) measurement with monoenergetic photons.

We now comment on the potentialities and shortcomings of the photo- and electronuclear reactions for the study of the giant resonances:

A - Photoabsorption. The total cross section [eqn.(1)] is dominated by the giant dipole resonance (GDR); it is difficult to study, in an inclusive measurement, the higher multipoles (L>1) because of the fixed and low momentum transfer. However, it should be noted that this very dominance is the basis for the usual decomposition into multipoles, and all electron data are essentially unanalyzable without complementary photon data. Furthermore, the availability of monoenergetic and/or polarized photon sources makes possible the study of the interference of the dominant E1 excitation with the M1 and E2 multipoles via angular-distribution studies. [We note in passing that the chief advantage of the (α,α') reaction is that it does not excite the isovector E1 mode to first order.]

B - Inelastic electron scattering. This was the first tool used[19] for the detection of the "new giant resonances", particularly the GQR. Here, one can vary the momentum transfer in order to sample giant multipole resonances of order L>1 and L=0 (the latter is forbidden for real photons). Alternately, by varying ω for a fixed q one obtains an excitation profile of the nucleus. However, with an (e,e') measurement one samples the strength function at $q \neq \omega$; hence, it is necessary to extrapolate the form factor back

to the photon point, and this is a long and difficult extrapolation (it is very hard to measure the form factor near q=ω; one is eventually beaten by the combination of the increase in the radiative corrections and the available running time). Also, without the detection of the decay product one cannot obtain complete information on the nature of the giant-resonance wave functions. And of course the large radiative back-ground constitutes an important experimental drawback.

C - Electrodisintegration. For such inclusive measurements, the cross section is expressed in terms of the well known virtual-photon formalism[2,20] as

$$\sigma_{e,x}(EL,E_e) = \int_0^{E_e} \sigma_{\gamma,x}(EL,\omega)\ N^{EL}(E_e,\omega)\ \frac{d\omega}{\omega} =$$

$$= (2\pi)^3\ \alpha\ \frac{(L+1)}{L[(2L+1)!!]^2} \int_0^{E_e} \frac{dB}{d\omega}(EL,\omega) \cdot \left[\frac{\Gamma_x(\omega)}{\Gamma}\right]_{EL} N^{EL}(E_e,\omega)\ \omega^{2L-2}\ d\omega \ . \qquad (10)$$

This is a sensitive tool for the study of E2 excitations because of the much greater intensity of the E2 virtual-photon spectrum relative to the E1 spectrum for high-Z nuclei (see, for example, Refs. 3, 4 and 20). Moreover, from the experimental point of view (e,f) measurements have a great advantage relative to (e,e') measurements, in that they are virtually background-free. The extracted E2 yield is proportional to an integral of the stregth function over all the final states of the scattered electron, with the advantage that the form factor falls so rapidly with q that its integral over q is dominated by events with q ≈ ω. The principal shortcomings are: a) it is necessary to solve an integral equation

by numerical methods in order to obtain the E2 strength function; b) it is necessary to know precisely the virtual-photon spectra, especially at low energies; and c) the experimental data must be of good quality and have adequate statistics down to the fission barrier.

D - Coincidence inelastic electron scattering. Because the (e,e'x) coincidence cross section is free in principle of nuclear backgrounds [in contrast to the (h,h'x) case where such backgrounds constitute the principal shortcoming] and because in (e,e'x) experiments it is possible to measure the energy and angular distributions associated with all the final states of the giant-resonance decay channels [which allow one to determine the multipolarities and the reaction mechanism unambiguously (see Ref. 21 for more details)], it is clear that (e,e'x) measurements have the potential of becoming the least uncertain way of studying the giant resonances and their decay channels. [A recent study of $^{12}C(e,e'p)$ has been carried out already[22)]]. However, here too, as in (e,e') measurements, it is necessary to extrapolate back to q=ω in order to extract the strength function. Also, low counting rates for such measurements, even with high-duty-cycle accelerators, frequently make these experiments very difficult and time-consuming.

2.4. Angular distributions

Measurement of the angular distribution of reaction products from a (γ,x) or (e,x) reaction enables one to extract information on the multipolar components of the nuclear transitions excited. With real photons, information on the E2 strength can be obtained from the angular-distribution coefficients of higher order than the $\cos^2\theta$ term in a Legendre expansion, and the M1 strength can be obtained with polarized photons. [For an (e,e'x) reaction, the virtual photons are already polarized because one has defined the scattering plane.] Because an (e,x) reaction is dominated by low-q, forward-angle electrons, the virtual photons are mostly transverse,

while those for an (e,e'x) reaction are mostly Coulomb (and hence longitudinal) at forward angles.

The angular distribution of electrofission fragments for a particular fission channel (J^π,K) is defined as[11]

$$\frac{d\sigma_e}{d\Omega_f}(J^\pi,K;E_e,\theta_f) = \sum_M \frac{\phi_e(J^\pi,K,M;E_e)}{2\pi} W^J_{MK}(\theta_f) \quad . \qquad (11)$$

For even-even nuclei (ground state $J^\pi=0^+$) $J^\pi=L^\pi$, where L is the multipolarity of the absorbed photon; K and M $(=0,\pm1,\pm2,\ldots,\pm L)$ are the projections of the nuclear angular momentum J on the symmetry axis of the nucleus and on the direction of the incident electron, respectively (see Fig.1); and $W^J_{MK}(\theta_f)$ is the angular-distribution function.

The coefficients of the angular distributions ϕ_e constitute the link between the electro- and photoexcitation processes and are given by[11]

$$\phi_e(J^\pi,K,M;E_e) = \int_0^{E_e} \sigma_{\gamma,f}(J^\pi,K;\omega)\, N^{(\lambda L,M)}(\omega,E_e)\, \frac{d\omega}{\omega} \qquad (12)$$

where $\sigma_{\gamma,f}(J^\pi,K;\omega)$ is the photofission cross section for the fission channel (J^π,K) and $N^{(\lambda L,M)}(\omega,E_e)$ is the virtual-photon spectrum (calculated in DWBA[20]) for a λL-transition with magnetic substate M. For electro- and photofission near the fission barrier the nuclear photoabsorption takes place in the energy region corresponding to the low-energy tails of the GDR and GQR; thus the cross sections reflect mainly the properties of the low-lying fission levels.

For electrofission angular distributions, following virtual-photon absorption of multipolarity L, one can differentiate easily between the lowest L-values involved ($L=0,1,2$, and 3), as

illustrated in Fig. 2. However, the (e,f) inclusive reactions for actinide nuclei are dominated by nuclear transitions having $L=1$ and 2, corresponding to excitations of the GDR and the GQR, respectively, because of the low q transferred to the nucleus. [In this regard we refer the reader to Ref. 4) for further details.]

From eqn. (11) one has

$$\frac{d\sigma_e}{d\Omega_f}(E_e,\theta_f) = \sum_{J^\pi=1^-,2^+} \sum_{K=0}^{\pm J} \frac{d\sigma_e}{d\Omega_f}(J^\pi,K;E_e,\theta_f) =$$

$$= A_e(E_e) + B_e(E_e)\sin^2\theta_f + C_e(E_e)\sin^2(2\theta_f) \qquad (13)$$

where the coefficient C_e, which contains contributions from the 2^+ levels only (in the absence of E3 and higher-multipolarity transitions), is given by[11]

$$C(E_e) = \frac{5}{32\pi}\int_0^{E_e}\left[3\sigma_{\gamma,f}(2^+,0;\omega) - 4\sigma_{\gamma,f}(2^+,1;\omega) + \sigma_{\gamma,f}(2^+,2;\omega)\right] N^{(E2,tot)}(\omega,E_e)\frac{d\omega}{\omega} \qquad (14)$$

and

$$N^{(E2,tot)}(\omega,E_e) = -\frac{3}{2}N^{(E2,0)}(\omega,E_e) + N^{(E2,1)}(\omega,E_e) - \frac{1}{4}N^{(E2,2)}(\omega,E_e) \qquad (15)$$

The E2 virtual-photon spectrum is dominated by the transverse component $(M=\pm1)$; only a small longitudinal component $(M=0)$ is present[11].

3. EXPERIMENTAL DETAILS AND DATA ANALYSIS

In the present work we have measured electrofission angular distributions for ^{234}U and analyzed them jointly with those for ^{236}U and ^{238}U. Also, we have computed the strength function for the fission decay channel of the GQR, for ^{234}U, ^{236}U, and ^{238}U, from the isoscalar E2 components of the photofission cross sections $\sigma_{\gamma,f}(E2,\omega)$ recently determined at this Laboratory[2-5]. The experimental technique and procedures were the same as for our previous work and are described at length in Refs. 4 and 11). However, in order to provide an overall view to the reader of the experimental and analytical uncertainties we include the following brief summary.

Figure 3 shows sketches of the three experimental arrangements used for these studies. The main possible sources of error are:

1) The beam monitoring device. This is a short-necked Faraday cup (FC) coupled directly to the reaction chamber, close to the target position. We have checked and found to be negligible a) the number of electrons scattered out of the FC owing to spreading of the beam by the target, b) the leakage current of the FC, and c) the degree of non-linearity of its response.

2) The beam characteristics. The beam spot size at the target position (diameter < 1 cm) is small compared either to the target size (diameter 4.45cm) or to the chamber radius (20cm), and there is negligible γ-ray contamination of the electron beam.

3) The fission-fragment detectors. These are mica foils, whose efficiency is 100%[11], and which subtended a modest solid angle (the average $\Delta\Omega_f \cong 5.7 \times 10^{-3}$ sr).

4) The uranium targets. These targets were thin (~200-300 $\mu g/cm^2$), and their uniformity was verified to ±2%; their absolute masses were determined by alpha counting. The bremsstrahlung produced in both the UO_2 targets and their thin (0.005 mm) titanium substrate was verified to be small and was accounted for by subtracting out an extrapolation of the bremsstrahlung-induced fission [as a function of the ratio of the radiator thickness to the total target thickness (in radiation lengths)].

5) Other backgrounds. Other backgrounds, resulting from room-returned neutrons and gammas, and scattered electrons, all were shown experimentally to be negligible.

The experimental procedures used to obtain the above-mentioned information are presented in detail in Refs. 4 and 11). A final check of the experimental conditions was obtained by measuring the bremsstrahlung-induced fission cross section σ_B as a function of the electron incident energy E_e, and comparing it to the quantity $\sigma_B^*(E_e) = \int_0^{E_e} \sigma_{\gamma,f}(\omega)\, N_B(E_e,\omega)\, d\omega$ where $\sigma_{\gamma,f}$ was obtained experimentally at Livermore[23] and N_B is the thin-target bremsstrahlung spectrum. The ratio σ_B/σ_B^* was found to be within a few percent of unity: 1.03 for ^{234}U and 1.04 for ^{236}U and ^{238}U.

We obtained the electrofission angular distributions $\frac{d\sigma_e}{d\Omega_f}$ [eqn. (11)] and the total electrofission cross section $\sigma_{e,f}(E_e) = \sum_{EL} \int_0^{E_e} \sigma_{\gamma,f}(EL,\omega)\, N^{EL}(E_e,\omega)\, \frac{d\omega}{\omega}$ from the experiments. Combining these two pieces of information with $\sigma_{\gamma,f}(\omega) = \sum_{EL} \sigma_{\gamma,f}(EL,\omega)$, one obtains information on the contributions from multipoles other than E1, that is, E2 and M1 [the justification for neglecting E0,E3,..., contributions, along with other details, are given in Ref. 4)]. It should be noted clearly that our method of data

analysis for E2 strength is based critically upon the knowledge of the virtual-photon spectra calculated in DWBA[20], in particular of N^{E1} and N^{E2}, which have been tested only at a level of accuracy of 10 to 20% [24,25].

The electrofission differential cross sections for ^{234}U, in the energy range from 5.5 to 25 MeV, were obtained by irradiating 255 $\mu g/cm^2$ targets of ^{234}U enriched to 99.1% with an electron beam from the University of São Paulo Linear Accelerator. The fission fragments were detected with mica-foil track detectors located at up to twelve different angles between 10^o and 100^o (eleven, usually, are plotted below; the twelfth, at 100^o, is redundant, and serves as an experimental check). The electrofission differential cross section $d\sigma_e/d\Omega_f$ is obtained from $d\sigma_e/d\Omega_f = (1/2\, N_t\, \phi)[N(\theta_f)/\Delta\Omega_f]$, where $N(\theta_f)$ is the number of fission tracks in a mica detector located at an angle θ_f (see Figs. 1 and 3), N_t is the number of target nuclei, ϕ is the number of electrons per cm^2, and $\Delta\Omega_f$ is the solid angle defined by the mica detector. The uncertainties in $d\sigma_e/d\Omega_f$, arising both from statistical fluctuations of $N(\theta_f)$ and from systematic uncertainties associated with N_t, ϕ, and $\Delta\Omega_f$, are typically ~5%. The resulting absolute total electrofission cross sections, allowing for uncertainties in the fitting procedure, should be accurate to ~7%. They are checked, furthermore, at roughly the 14% level by the ratio σ_B/σ_B^*, to be within 4% of the $\sigma(\gamma,f)$ results of Ref. 23), which are themselves quoted to be accurate to within 7% (but with a possible 10% uncertainty in the calculation of N_B).

4. RESULTS AND THEIR INTERPRETATION

4.1. Angular-distribution results

An angular distribution having the form given by eqn.(13) has been assumed, and the coefficients A,B,C were obtained by least-squares fitting to the experimental $d\sigma_e/d\Omega_f$ data. Figure 4 shows the electrofission differential cross sections for ^{234}U for values of E_e between 5.5 and 12.7 MeV where the anisotropies are large; above ~13 MeV the anisotropies are small and have large fractional uncertainties. The solid curves in Figure 4 were obtained as least-squares fits of $A+B\sin^2\theta_f+C\sin^2(2\theta_f)$ to the experimental points; it should be noted that both the experimental points and the curves have been divided by A (the isotropic coefficient) in order to make clear the actual size of the anisotropy. Similar figures for ^{236}U and ^{238}U appear in Refs. 4) and 2), respectively. Figures 5A, 5B and 5C show the normalized coefficients a,b and c, defined as the A,B and C coefficients divided by $[2A+(4/3)B+(16/15)C]$, respectively; this latter quantity is proportional to the total electrofission cross section. It is clear from Fig.5C that the E2 contribution to the electrofission process is significant well above the fission barrier, in contrast with the photofission case where the E2 anisotropy is nearly equal to zero at energies $\gtrsim$ 9 MeV. In this regard we note that in a recent electrofission study of ^{238}U J.Aschenbach et al.[26] obtained values for c in excellent agreement with those from the present work.

4.2. Strength functions for the fission decay of the GQR

Figure 6 shows the strength distributions of the GQR fission decay for ^{234}U, ^{236}U, and ^{238}U, obtained from the values for $\sigma_{\gamma,f}(E2,\omega)$ of Refs. 2, 4 and 5) (see Sec.2.1), using the definition given by eqn.(1). It is worth remembering that in the three-dimensional space (S^L,q,ω) in which the nuclear response surface $S^L \equiv S^L(q,\omega)$ is defined, the contour of S^L projected onto the plane $q=\omega$ is given by the strength function [see eqn.(9)]. It

is important to observe in Fig.6 that the peaks and widths of the E2 strength functions are quite different from those resulting simply from the previously published values for $\sigma_{\gamma,f}(E2,\omega)$. All the existing results for the actinide nuclei are listed in Table 1, where the strength-function parameters deduced from the electrofission results (after correction for second-chance fission) are compared with those obtained from hadron-induced fission.

Studies of the fragmentation of the GQR in deformed nuclei have been performed in the framework of various models, most recently by Abgrall et al.[15], who used an adiabatic cranking assumption. Shown in Fig. 6 for illustrative purposes is the distribution of the quadrupole strength for a well-deformed nucleus ($\beta \approx 0.3$) with coupled α, β, and γ vibrations [see Ref. 15) for details]. The largest fraction of the E2 strength (59%) is located near 9 MeV ($56 \times A^{-1/3}$ MeV), in qualitative agreement with the present results. Also indicated in Fig. 6 are the positions of the peaks of the E2 strength (at ~6 and 8.8 MeV) obtained from preliminary (e,e'f) coincidence results for ^{238}U (Ref. 6)). These results are seen to be in excellent agreement with the present ones.

On the other hand, it is very hard to find a reasonable way to reconcile the hadron- with the electron-scattering results; the reason is simply that the E2 strength deduced from the hadron-induced reactions for actinide nuclei (see table 1), peaks at ~11 MeV and vanishes at energies below ~8 MeV. This disappearance of fission strength below 8 MeV illustrates the principal shortcoming of the hadron-scattering measurements, namely, the uncertainty in the subtraction of the (real) nuclear background. Figure 7 compares the results obtained from the $^{238}U(\alpha,\alpha'f)$ measurement of Ref. 8) and those from the electrofission work of Refs. 2 and 3). Part of the motivation for

the detailed measurement and analysis of the electrofission-fragment angular distributions just above the fission barrier presented here was so that one could be sure about the appreciable fraction of the total E2 strength concentrated close to the fission barrier (in contrast with the zero E2 strength observed there in the hadron experiments).

4.3. E2 strength functions for the low-lying K=0 and K=1 fission channels

A simple visual inspection of Fig. 4 reveals the presence of a major E2 component in the electrofission cross section, at least at low energies, as indicated by the systematic enhancement found in $d\sigma_e/d\Omega_f$ near 50^o. A more detailed analysis can be performed by means of the coefficient C in particular [eqn.(3)] of the angular distributions (because it represents contributions from E2 transitions alone) to give the fission decay from the low-lying levels $(2^+,0)$, $(2^+,1)$, and $(2^+,2)$ of the transition nucleus (at the saddle point).

Figure 8 displays the C coefficient (in mb/sr) obtained here for ^{234}U and from previous work[4,11] for ^{236}U and ^{238}U. The fission strength functions $\sum_K \frac{dB}{d\omega}(E2) \cdot \frac{\Gamma_f}{\Gamma}(2^+,K)$ (in $fm^4.MeV^{-1}$) which were obtained from the E2-photofission cross sections after subtraction of an approximation to the contribution resulting from second-chance fission[3-5] (and shown in Fig. 6 up to 15 MeV) are also plotted in Fig. 8. If the photon energy $\omega \leq [B_f(2^+) + \Delta]$, where $B_f(2^+)$ is the 2^+ fission barrier and Δ is the pairing gap, then the K-values appearing in the above summation are representative only of the corresponding rotational bands (and are dominated by the K=0 and K=1 bands). At the low-energy tail of the GQR the strength function $dB/d\omega$ varies in general, with ω, and therefore the behavior of $\left[\frac{dB}{d\omega}(E2;\omega) \cdot \frac{\Gamma_f}{\Gamma}(2^+,K;\omega)\right]$ as a function of ω

reflects the main trend of the fission probabilities associated with the low-lying fission levels $(2^+,K)$. From the experimentally determined C coefficients of the electrofission angular distributions it is possible to study the competition between the $(2^+,0)$ and $(2^+,1)$ fission channels and thus to obtain information about the fraction of the E2 strength concentrated in each of these fission channels. The solid curves in Fig.8 were obtained by numerical integration of

$$\frac{15}{32\pi}\int_0^{E_e}\sigma^{E2}_{\gamma,f}(\omega)\;N^{(E2,tot)}(E_e,\omega)\;\frac{d\omega}{\omega}\;\equiv\;C'(E_e) \qquad (16)$$

using the experimentally determined $\sigma^{E2}_{\gamma,f}$ from Refs. 2, 4, and 5). Comparing eqns. (14) and (16) we see that C=C' if $\sigma_{\gamma,f}(2^+,0) = \sigma^{E2}_{\gamma,f}$, that is, in a situation where the K=0 channel is the only one open to fission. More generally, one has

$$\sigma^{E2}_{\gamma,f}(\omega) \;=\; \sum_{K=0}^{2}\sigma_{\gamma,f}(2^+,K;\omega) \qquad (17)$$

The opening of the K=1 channel causes a diminution of the cross-section kernel of the integral C [eqn.(14)] and as a consequence results in a change of its slope, as shown in Fig. 8 by the dashed curves. Therefore the comparison of C and C' clearly establishes the energy $B_f(2^+,1)$ corresponding to the location of the fission barrier for the $(2^+,1)$ level. [It should be noted that it is virtually impossible to detect the $(2^+,1)$ level in photofission angular-distribution experiments (with unpolarized photons).] The shaded bands in Fig.8 represent the energy limits for $B_f(2^+,1)$, deduced from C and C'. The locations of $B_f(2^+,0)$ were assigned simply from consideration of the concentration of the E2 strength below $B_f(2^+,1)$. The structures observed in $\frac{dB}{d\omega}(E2)\cdot\frac{\Gamma_f}{\Gamma}(2^+)$ near 6 MeV result partly from the locations of

the $(2^+,0)$ levels and partly from the neutron-emission competition; it should be noted here that an E2 structure has been observed near 6 MeV in the preliminary $^{238}U(e,e'f)$ coincidence data of Ref. 6). The arrows in Fig. 8 indicate the results obtained from the photofission studies of Ref. 13). These results are listed, along with the conclusions of the present work, in Table 2; it can be seen that good agreement has been obtained both for the determination of the values for $B_f(2^+,0)$ and for the overall $(2^+,0)$ strength as well.

Finally, we show another way to see explicity the [K=0] - [K=1] competition for the E2 fission. From eqns.(14), (15), and (16) (for K=0 and K=1) it is straightforward to obtain

$$\frac{C(E_e) + (4/3)C'(E_e)}{(8/3)C'(E_e)} = \frac{\int_0^{E_e}\sigma_{\gamma,f}(2^+,0;\omega)\;N^{(E2,tot)}(E_e,\omega)\frac{d\omega}{\omega}}{\int_0^{E_e}\left[\sigma_{\gamma,f}(2^+,0;\omega) + \sigma_{\gamma,f}(2^+,1;\omega)\right]N^{(E2,tot)}(E_e,\omega)\frac{d\omega}{\omega}} \equiv$$

$$\equiv \frac{[K=0]}{[K=0] + [K=1]}\quad , \qquad (18)$$

which represents the relative participation of the K=0 E2 fission channel to the entire process, as illustrated in Fig. 9 for ^{234}U, ^{236}U, and ^{238}U. Here, one can distinguish (with some uncertainty) two energy regions, one where the [K=0]-to-total ratio is $\gtrsim 1$ and one where it is <1; thus, the boundary between these two regions indicates the opening of the K=1 fission channel for E2 excitation (the shaded bands are from Fig. 8).

4.4. E2 fission probabilities near the barrier

We have calculated the E2 relative fission proba-

bilities $\left[\frac{\Gamma_f(\omega)}{\Gamma}\right]_{E2}$ for ^{234}U, ^{236}U, and ^{238}U, as a function of the excitation energy, by dividing the fission strength shown in Fig. 6 by a strength function $\frac{dB}{d\omega}(E2,\omega)$ for the photoabsorption process which is assumed to have a Breit-Wigner shape with its peak energy and width equal to those for the fission strength functions (Table 1), and its area exhausting one E2 energy-weighted sum-rule unit. In Table 3 are shown the present results, together with those obtained from recent photofission data[23] (the latter represent mostly E1 contributions). The fission process is strongly favored in the decay of the GQR, for these actinide nuclei, whereas neutron evaporation is favored in the decay of the GDR (see also Ref. 5)), particularly at excitation energies close to the fission barrier.

In order to understand the difference between the fission decay of actinide nuclei following E1 and E2 excitation we note that: a) the neutron binding energy B_n is the same for both processes; therefore, it plays no role; and b) for excitation energies below $B_f+\Delta$ ($\cong$ 7 MeV) it is possible to reproduce (through standard statistical calculations) the experimental values obtained for $P_f(E2)$; this is achieved because of the fact that the 2^+ fission-barrier heights are considerably lower than the values for B_n, whereas the 1^- barrier heights are much closer to the B_n values [more details can be found in Ref. 3)]. However, for energies $>B_f+\Delta$, where intrinsic excitations become increasingly important, it would be expected that $P_f(E2) \cong P_f(E1)$= the fission probability of the compound nucleus, but that is not the case (see Table 3). It is possible to speculate that direct fission would be facilitated for E2 excitations, but it appears to be unlikely that the isoscalar GQR amplitude is sufficiently large to result in a large direct-fission component.

5. SUMMARY AND CONCLUSIONS

The measured electrofission angular distributions for ^{234}U were analyzed together with those for ^{236}U and ^{238}U (from previous studies performed at this Laboratory). The energy positions for the K=0 and K=1 fission barriers and the competition between these fission channels following E2 excitation for these nuclei have been delineated. The E2 fission strength functions were extracted from the E2 photofission cross sections for ^{234}U, ^{236}U, and ^{238}U. The total amount of E2 fission strength concentrated in the K=0 channel near the barrier is substantial, and is in good agreement with earlier photofission angular-distribution data. We estimate the E2 fission probabilities $P_f(E2)$ for ^{234}U, ^{236}U, and ^{238}U, at energies below the pairing gap; these results also agree with standard statistical calculations, and show that $P_f(E2)$ is very sensitive to the location of the E2 fission barrier.

Finally, the present results stand in sharp contrast with those obtained for the hadron-induced fission of ^{238}U in the energy region of the GQR, where no E2 fission strength was detected at energies $\lesssim$ 8 MeV.

ACKNOWLEDGMENTS

We are indebted to Prof.U.Kneissl and especially to Prof. L.S.Cardman for their careful reading of the manuscript and their valuable comments and suggestions thereon.

REFERENCES

1) G.J. Wagner, Proc. Giant Multipole Topical Conf., Oak Ridge, 1979, in Nuclear Science Research Conference Series V.1, p. 251, edited by F.E. Bertrand (Harwood Academic Publishers).

2) J.D.T. Arruda-Neto, S.B. Herdade, B.S. Bhandari, and I.C. Nascimento, Phys. Rev. C18 (1978) 863.

3) J.D.T. Arruda-Neto and B.L. Berman, Nucl. Phys. A349 (1980) 483.

4) J.D.T. Arruda-Neto, B.L. Berman, S.B. Herdade, and I.C. Nascimento, Phys. Rev. C22 (1980) 1996.

5) J.D.T. Arruda-Neto, B.L. Berman, S.B. Herdade, and I.C. Nascimento, Phys. Rev. C23 (1981) 2595.

6) J.R. Calarco, J.D.T. Arruda-Neto, K. Griffioen, S.S. Hanna, D. H.H. Hoffmann, R.E. Rand, K. Wienhard, and M.R. Yearian, private communication.

7) J. van der Plicht, M.N. Harakeh, A. van der Woude, P. David, and J. Debrus, Phys. Rev. Lett. 42 (1979) 1121 ; J. van der Plicht, M.N. Harakeh, A. van der Woude, P. David, J. Debrus, H. Janszen, and J. Schulze, Nucl. Phys. A346 (1980) 349.

8) F.E. Bertrand, J.R. Beene, C.E. Bemis, Jr., E.E. Gross, D.J. Horen, J.R. Wu, and W.P. Jones, Phys. Lett. 99B (1981) 213.

9) A.C. Shotter, C.K. Gelbke, T.C. Awes, B.B. Back, J. Mahoney, T.J.M. Symons, and D.K. Scott, Phys. Rev. Lett. 43 (1979) 569.

10) S.S. Hanna, Int. School of electro- and photonuclear reactions, Erice, Italy (1976), in Lecture Notes in Physics (Springer, Berlin) 61 (1977) 275.

11) J.D.T. Arruda-Neto, S.B. Herdade, and I.C. Nascimento, Nucl. Phys. A334 (1980) 297.

12) B.S. Bhandari and I.C. Nascimento, Nucl. Sci. Eng. 60 (1976) 19.

13) L.J. Lindgren, A. Alm, and A. Sandell, Nucl. Phys. A298 (1978) 43.

14) R. Vandenbosch and J.R. Huizenga, Nuclear Fission, (Academic Press, N.Y.,1973), chapter V.

15) Y. Abgrall, B. Morand , E. Caurier, and B. Grammaticos, Nucl. Phys. A346 (1980) 431.

16) J.S. O'Connell, Proc. Int. Conf. on photonuclear reactions and applications, ed. B.L. Berman (Lawrence Livermore Laboratory, Livermore, Calif., 1973), p.71, and references therein.

17) H. Überall, Electron Scattering from Complex Nuclei (New York, Academic Press, 1971), p.522.

18) T.W. Donnelly and J.D. Walecka, Ann. Rev. Nucl. Sci. 25 (1975) 329.

19) R. Pitthan and Th. Walcher, Phys. Lett. 36B (1971) 563; Z. Naturforsch. 27a (1972) 1683.

20) W.W. Gargaro and D.S. Onley, Phys. Rev. C4 (1971) 1037.

21) J.S. O'Connell, "Electromagnetic Coincidence Experiments"; contribution to the June 1977 MIT Workshop on Intermediate Energy Electromagnetic Interactions with Nuclei.

22) J.R. Calarco, J. Arruda-Neto, K. Griffioen, S.S. Hanna, D. Hoffmann, M. Mueller, B. Neyer, M. O'Halloran, R. Rand, K. Wienhard, and M.R. Yearian, in Workshop on Nuclear Structure with Medium Energy Probes, LASL, Los Alamos, 1980.

23) J.T. Caldwell, E.J. Dowdy, B.L. Berman, R.A. Alvarez, and P. Meyer, Phys. Rev. C21 (1980) 1215, and private communication for the ^{234}U data.

24) I.C. Nascimento, E. Wolynec, and D.S. Onley, Nucl. Phys. A246 (1975) 210.

25) J.D.T. Arruda-Neto, B.L. Berman, S.B. Herdade, and I.C. Nascimento, Phys. Rev. C22 (1980) 1794.

26) J.Aschenbach, R.Haag , and H.Krieger, Z.Physik A292 (1979) 285.

TABLE 1

First-chance fission-decay parameters of the GQR strength function*

Nucleus	Reaction	Peak energy (MeV)	FWHM (MeV)	EWSR (%)	$P_f(E2)$ (%)	Ref.
^{234}U	(e,f)	8.2 ± 0.4	4.8 ± 1.0	87 ± 14	70 ± 15 a)	this work
^{236}U	(e,f)	8.9 ± 0.4	4.7 ± 1.0	72 ± 10	60 ± 10 a)	this work
^{238}U	(e,f)	8.3 ± 0.4	5.0 ± 1.0	55 ± 10	40 ± 10 a)	this work
^{238}U	(e,e'f)	8.8 ± 0.2	~3/4.5 ± 0.5 b)	___ c)	___ c)	6
^{238}U	(α,α'f)	~11 d)	4.0 ± 0.5 d)	—	< 10	7
^{238}U	(α,α'f)	10.6	2.2 ± 0.2 e)	—	25 ± 10	8
^{238}U	(^6Li,^6Li'f)	~10.5	~7 d)	—	≥20	9

* In our early work we published[2,4,5] results derived simply from the cross sections and not the parameters of the strength functions obtained therefrom.

a) As determined at the peak energy.

b) Without and with the inclusion of the peak at ~6 MeV, respectively.

c) No definitive figures at the present stage of the data analysis can be given but they are at least equivalent to the (γ,f) results[23] for GDR fission decay at ~9 MeV, and larger near ~6 MeV.

d) From the published singles spectrum.

e) For the K=0 component only (see Ref. 8)).

TABLE 2

E2 strength concentrated in the $(2^+,0)$ fission channel and the 2^+ fission-barrier heights

Nucleus	E2 strength (%) $(J^\pi,K) = (2^+,0)$ a)		$B_f(2^+,0)$ (MeV)		$B_f(2^+,1)$ (MeV)
	b)	c)	b)	c)	b)
^{234}U	10 ± 2	16 ± 3	6.0 to 6.4	5.4 to 6.2	≥6.7
^{236}U	13 ± 2	8 ± 2	5.5 to 6.0	5.6 to 6.0	≥6.4
^{238}U	6 ± 1	7 ± 1	5.8 to 6.2	5.8 to 6.2	≥6.7

a) $\frac{1}{B(E2)} \int \frac{dB}{d\omega}(E2,\omega) \frac{\Gamma_f}{\Gamma}(2^+,0)\, d\omega \times 100$, where B(E2) is equal to one E2 energy-weighted sum-rule unit.

b) Present work.

c) Derived from the cross sections published in Ref. 13).

TABLE 3

E1 and E2 fission probabilities

Nucleus	$P_f(E2)$ near[a] (%) 6 MeV	Stat. Calc. for $P_f(E2)$ near[a] 6 MeV	Parameters[b] B_n ; $B_f(2^+,0)$	$P_f(E2)$ near[a] (%) 9 MeV	$P_f(E1)$ near[a] (%) 9 MeV [c]
^{234}U	~100	100	6.84 ; 6.00	70 ± 15	~45
^{236}U	80 ± 10	95	6.55 ; 5.90	60 ± 10	~35
^{238}U	90 ± 10	90	6.15 ; 5.75	40 ± 10	~25

a) "near" means in an interval ~1 MeV wide.

b) Parameters (in MeV) used for statistical calculations of $P_f(E2)$, where $B_f(2^+,0)$ is the fission-barrier height for the level $(J^\pi,K) = (2^+,0)$ at the saddle point.

c) From Ref. 23).

FIGURE CAPTIONS

FIG. 1 - Kinematics for an (e,e'f) reaction, showing the nuclear angular momentum J and its projections on the z-axis (laboratory frame of reference) and on the nuclear symmetry axis (along the fission-fragment direction); the other symbols are defined in the text.

FIG. 2 - K=0 photofission angular distributions for dipole (L=1), quadrupole (L=2) , and octupole (L=3) photon absorption by an even-even nucleus.

FIG. 3 - Schematic diagrams of the experimental arrangements for electrofission angular-distribution measurements (top), electrofission yield measurements (for 2π geometry) (middle), and bremsstrahlung-induced fission (also for 2π geometry) (bottom).

FIG. 4 - Electrofission-fragment angular distributions $\frac{1}{A_e(E_e)} \frac{d\sigma}{d\Omega_f}(E_e,\theta_f)$ for ^{234}U , for incident electrons having energies from 5.5 to 12.7 MeV. The curves are least-squares fits of the function defined in eqn.(13) to the experimental points. Both systematic and statistical uncertainties are included in the error flags (and were used in the fitting procedure).

FIG. 5A - Coefficient A of the angular-distribution function [eqn.(13)] divided by the quantity $[2A + (4/3)B + (16/15)C]$ (which is proportional to the total electrofission cross section), as a function of the incident electron energy.

FIG. 5B - Same as in Fig. 5A, for the coefficient B .

FIG. 5C - Same as in Fig. 5A, for the coefficient C .

FIG. 6 - Experimentally determined fission strength functions $\frac{dB}{d\omega}\cdot\frac{\Gamma_f}{\Gamma}$ for the GQR for the even uranium isotopes, derived from the (e,f) cross sections. The error flags shown on the curve for ^{234}U (which are the same percent errors associated with the cross sections $\sigma_{\gamma,f}(E2,\omega)$ [2,4,5] used in the present derivation of the strength-function curve) are roughly the same as those for ^{236}U and ^{238}U. The shaded bands represent the fragmentation of the GQR, as explained in the text and in Ref. 15). The arrows indicate the energy of the structures in the E2 strength as determined from (e,e'f) and (h,h') experiments for ^{238}U (see text).

FIG. 7 - E2 strength function for ^{238}U, labeled "(e,f)", from the present study (also shown in Fig. 6), and the one from the $(\alpha,\alpha'f)$ measurement of Ref. 8). The $(\alpha,\alpha'f)$ curve has been normalized at the peak of the E2 strength for comparison purposes.

FIG. 8A - Absolute values for the coefficient of the $\sin^2(2\theta_f)$ term in the electrofission differential cross section $C(E_e)$ [eqn.(13)], obtained from the measured angular distributions for ^{234}U (data points, scale on left), along with $\sum_K \frac{dB}{d\omega}(E2)\cdot\frac{\Gamma_f}{\Gamma}(2^+,K)$ over the same energy range (solid curve, scale on right). The solid curve C' is defined in the text. The shaded bands (whose widths represent the uncertainty in their determination) and arrows represent the location of the fission barriers as determined in this work and in Ref. 13), respectively.

FIG. 8B - Same as in Fig. 8A, for ^{236}U.

FIG. 8C - Same as in Fig. 8A, for ^{238}U.

FIG. 9 - Competition between the $(2^+,0)$ and $(2^+,1)$ fission channels [as defined in eqn.(18)].

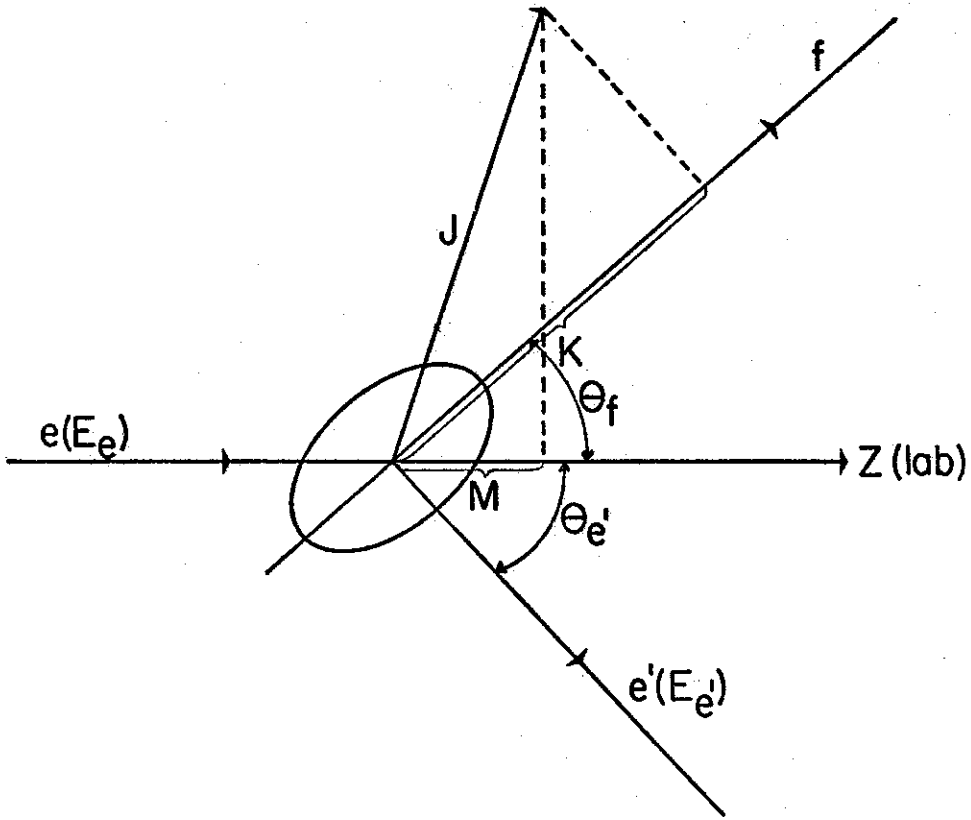
f
J
K
Θ_f
e(E_e)
Z (lab)
M
$\Theta_{e'}$
e'($E_{e'}$)

Fig. 1

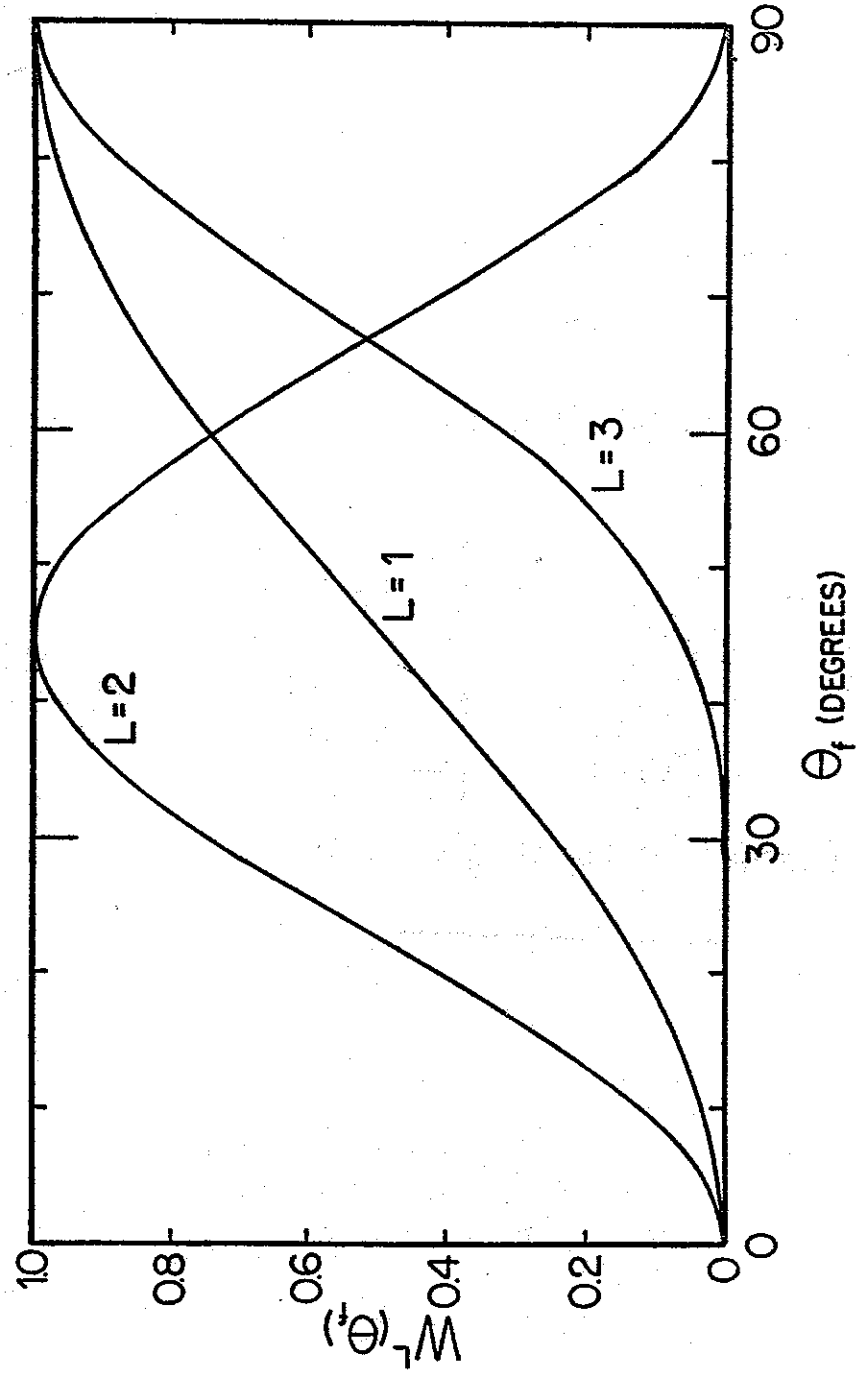
L=2
L=1
L=3
$W_L(\Theta_f)$
1.0
0.8
0.6
0.4
0.2
0
30
60
90
Θ_f (DEGREES)

Fig. 2

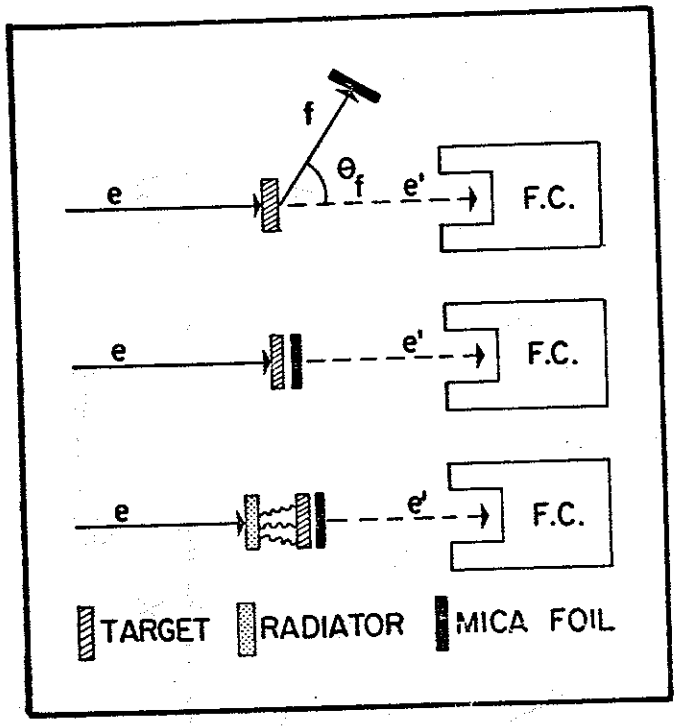
f
θ_f
e
e'
F.C.
e
e'
F.C.
e
e'
F.C.
TARGET
RADIATOR
MICA FOIL

Fig. 3.

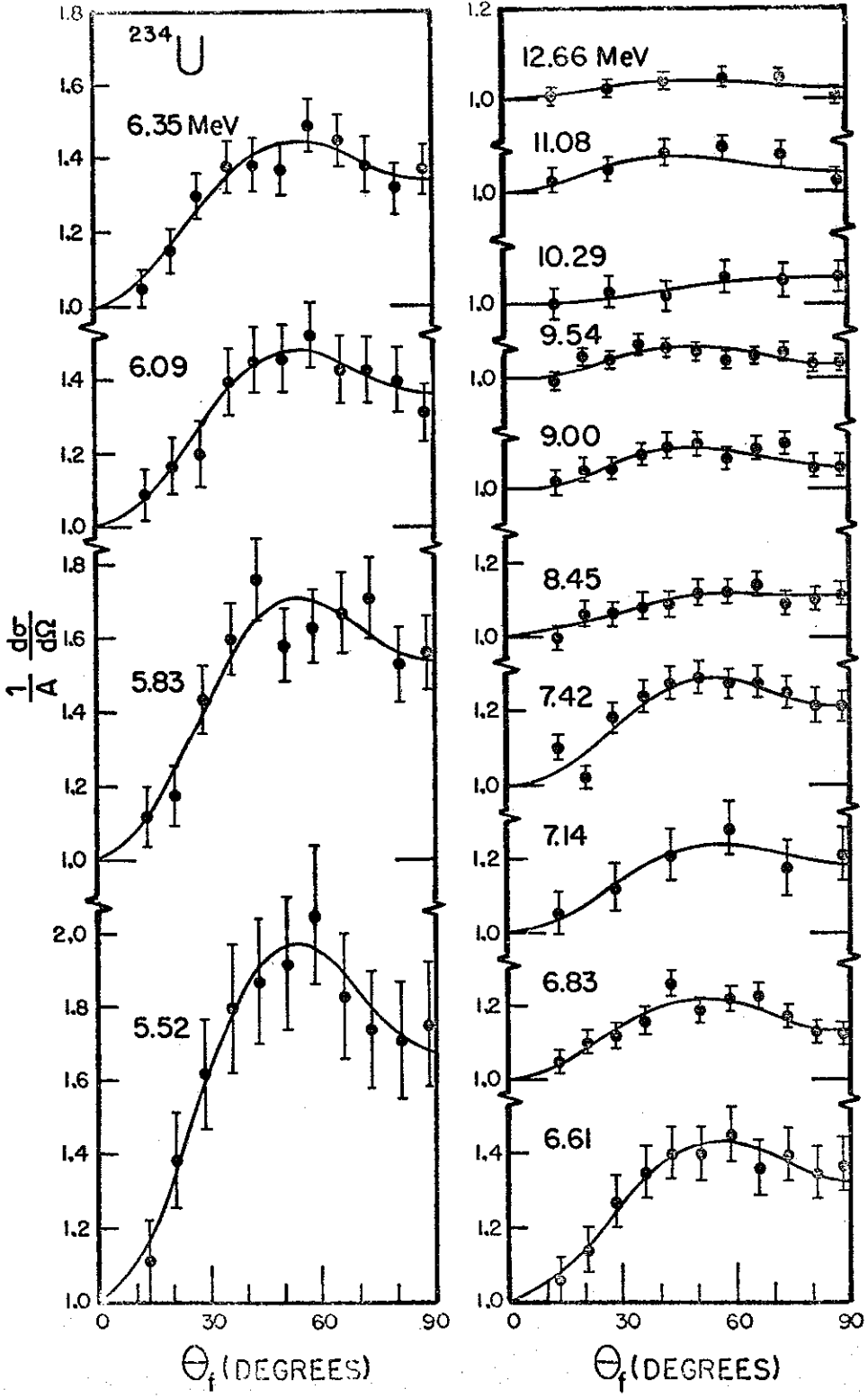
^{234}U
6.35 MeV
6.09
5.83
5.52
12.66 MeV
11.08
10.29
9.54
9.00
8.45
7.42
7.14
6.83
6.61
$\frac{1}{A}\frac{d\sigma}{d\Omega}$
θ_f (DEGREES)
θ_f (DEGREES)

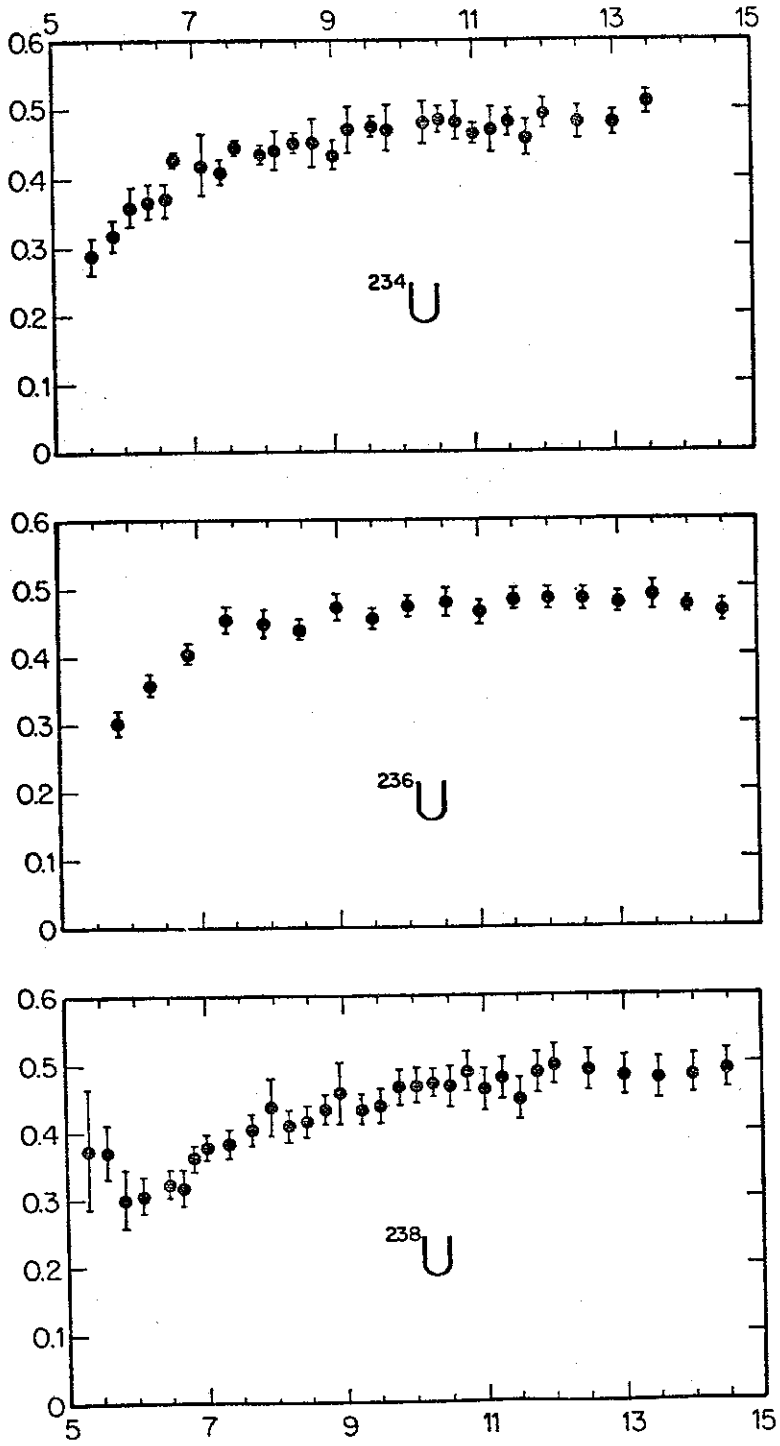
234U
236U
238U
ELECTRON ENERGY (MeV)

Fig. 5A

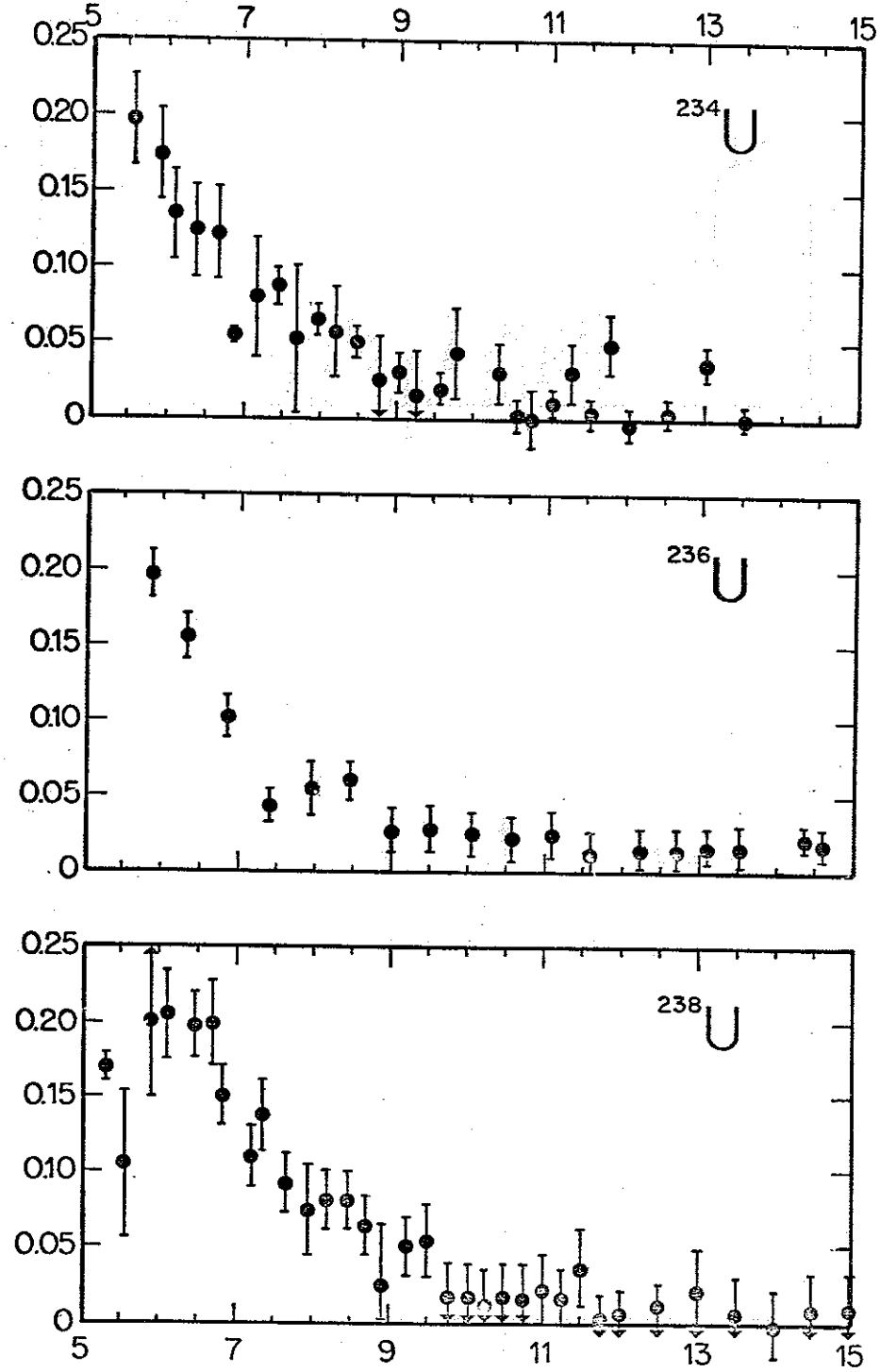
234U
236U
238U
ELECTRON ENERGY (MeV)

Fig. 5B

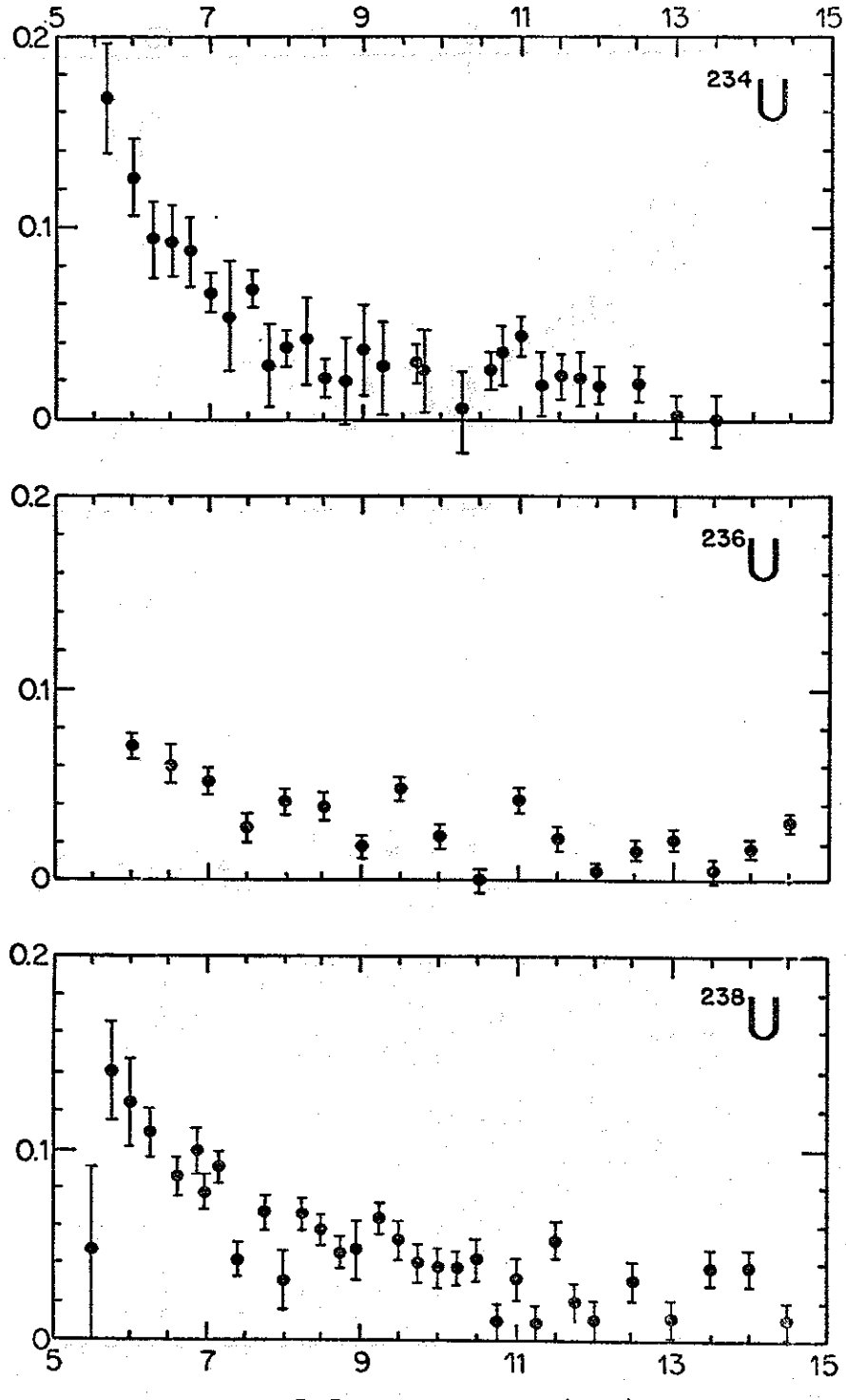
234U
236U
238U
0.2
0.1
0
5
7
9
11
13
15
ELECTRON ENERGY (MeV)

Fig. 5c

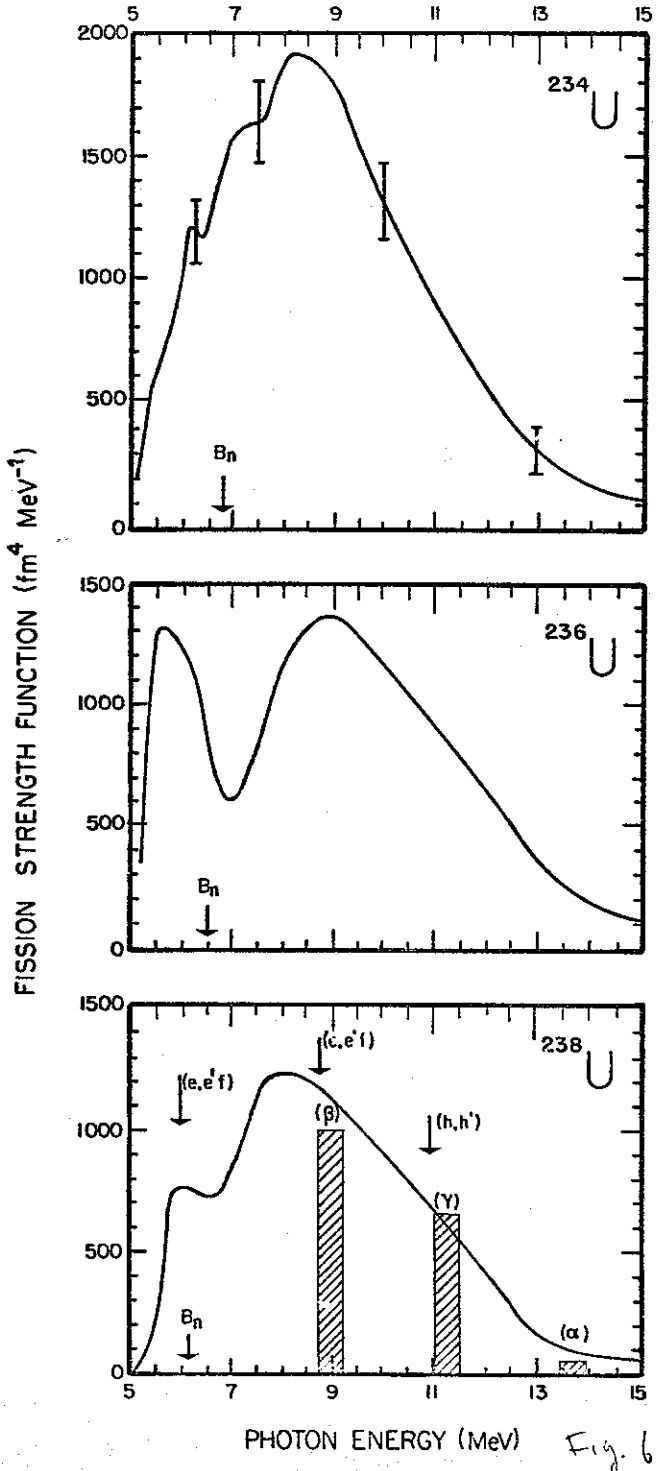
234U
236U
238U
Bn
(e,e'f)
(c,e'f)
(h,h')
(β)
(γ)
(α)
2000
1500
1000
500
0
5
7
9
11
13
15
FISSION STRENGTH FUNCTION (fm4 MeV-1)
PHOTON ENERGY (MeV)

Fig. 6

Fig. 7

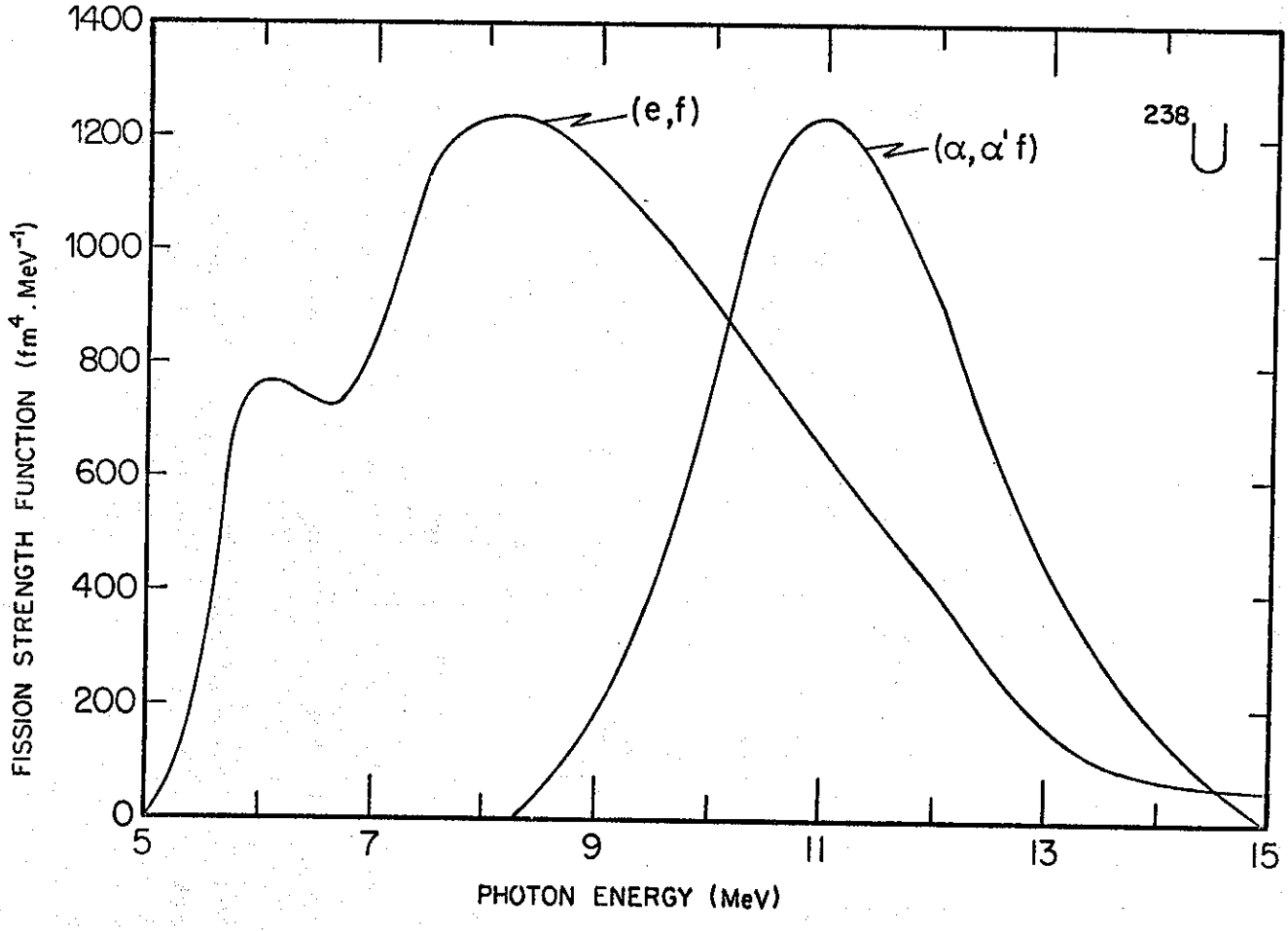
1400
1200
1000
800
600
400
200
0
5
7
9
11
13
15
(e,f)
(α, α' f)
238 U
FISSION STRENGTH FUNCTION (fm⁴.MeV⁻¹)
PHOTON ENERGY (MeV)

Fig. 8A

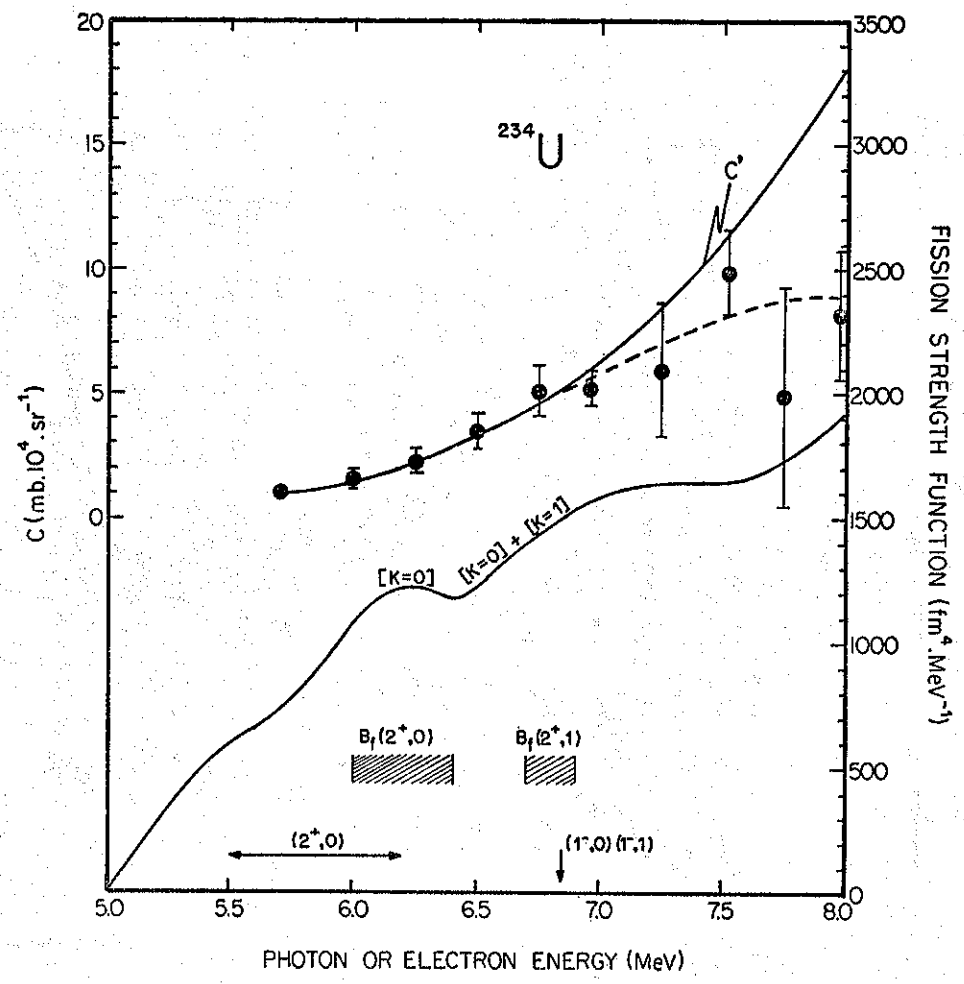
20
15
10
5
0
3500
3000
2500
2000
1500
1000
500
0
234 U
C'
[K=0]
[K=0] + [K=1]
B_f(2⁺,0)
B_f(2⁺,1)
(2⁺,0)
(1⁻,0) (1⁻,1)
5.0
5.5
6.0
6.5
7.0
7.5
8.0
C (mb.10⁴.sr⁻¹)
FISSION STRENGTH FUNCTION (fm⁴.MeV⁻¹)
PHOTON OR ELECTRON ENERGY (MeV)

Fig. 8B

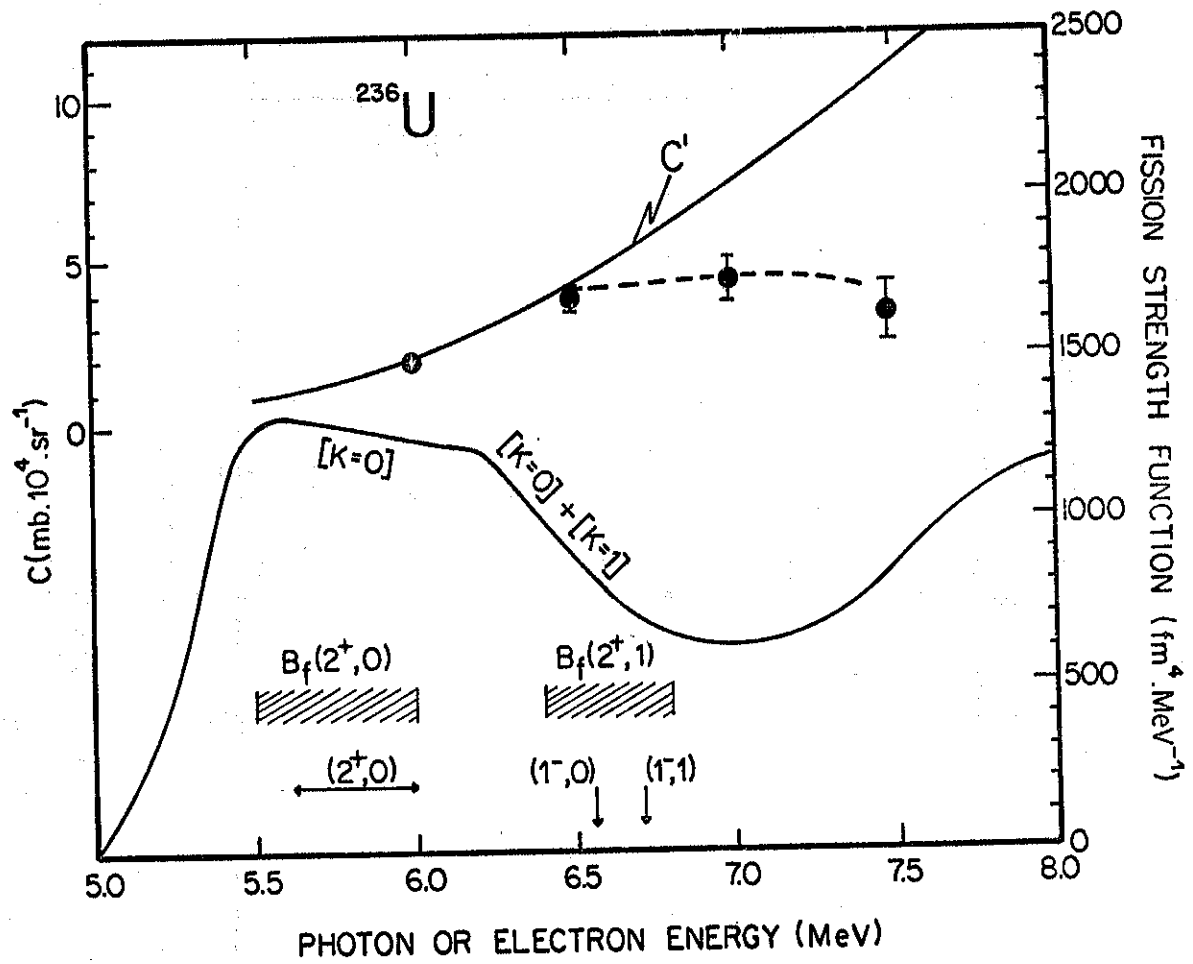
^{236}U
C'
[K=0]
[K=0] + [K=1]
$B_f(2^+,0)$
$B_f(2^+,1)$
$(2^+,0)$
$(1^-,0)$
$(1^-,1)$
C(mb.10^4.sr^{-1})
FISSION STRENGTH FUNCTION (fm^4.MeV^{-1})
PHOTON OR ELECTRON ENERGY (MeV)
10
5
0
2500
2000
1500
1000
500
0
5.0
5.5
6.0
6.5
7.0
7.5
8.0

Fig. 8C

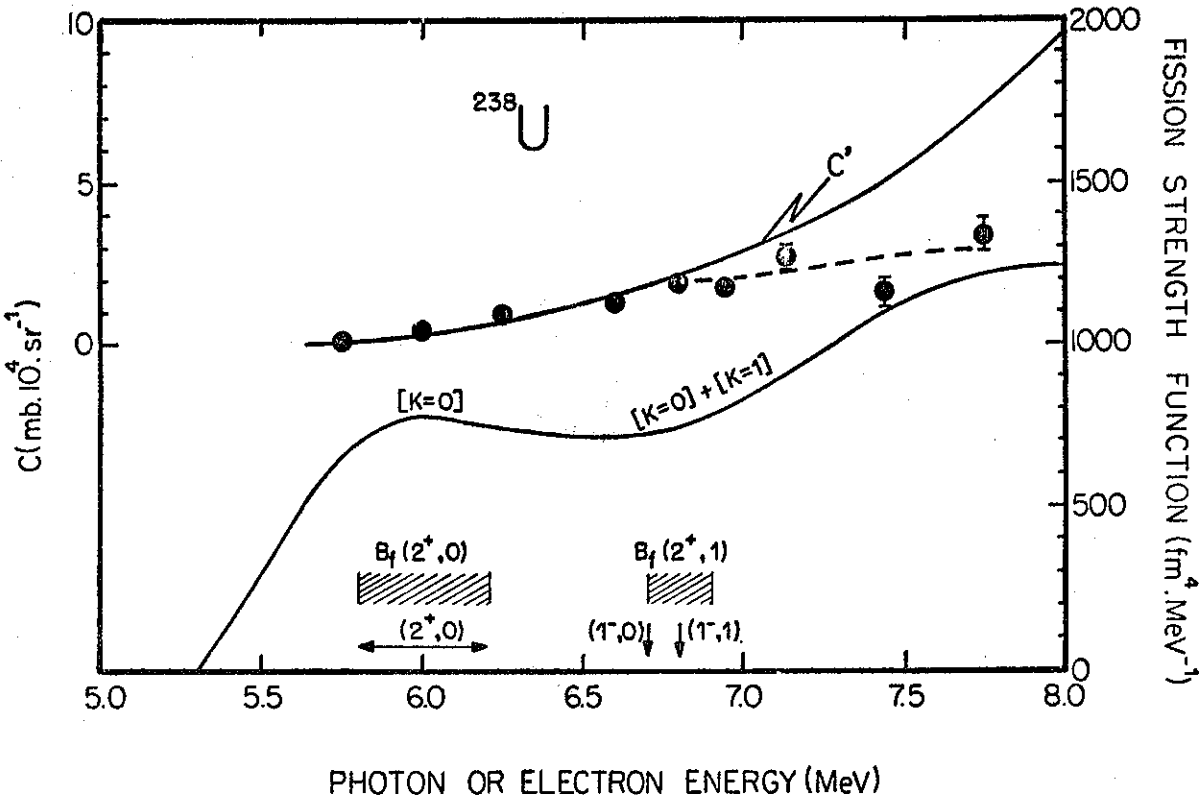
^{238}U
C'
[K=0]
[K=0] + [K=1]
$B_f(2^+,0)$
$B_f(2^+,1)$
$(2^+,0)$
$(1^-,0)$
$(1^-,1)$
C(mb.10^4.sr^{-1})
FISSION STRENGTH FUNCTION (fm^4.MeV^{-1})
PHOTON OR ELECTRON ENERGY (MeV)
10
5
0
2000
1500
1000
500
0
5.0
5.5
6.0
6.5
7.0
7.5
8.0

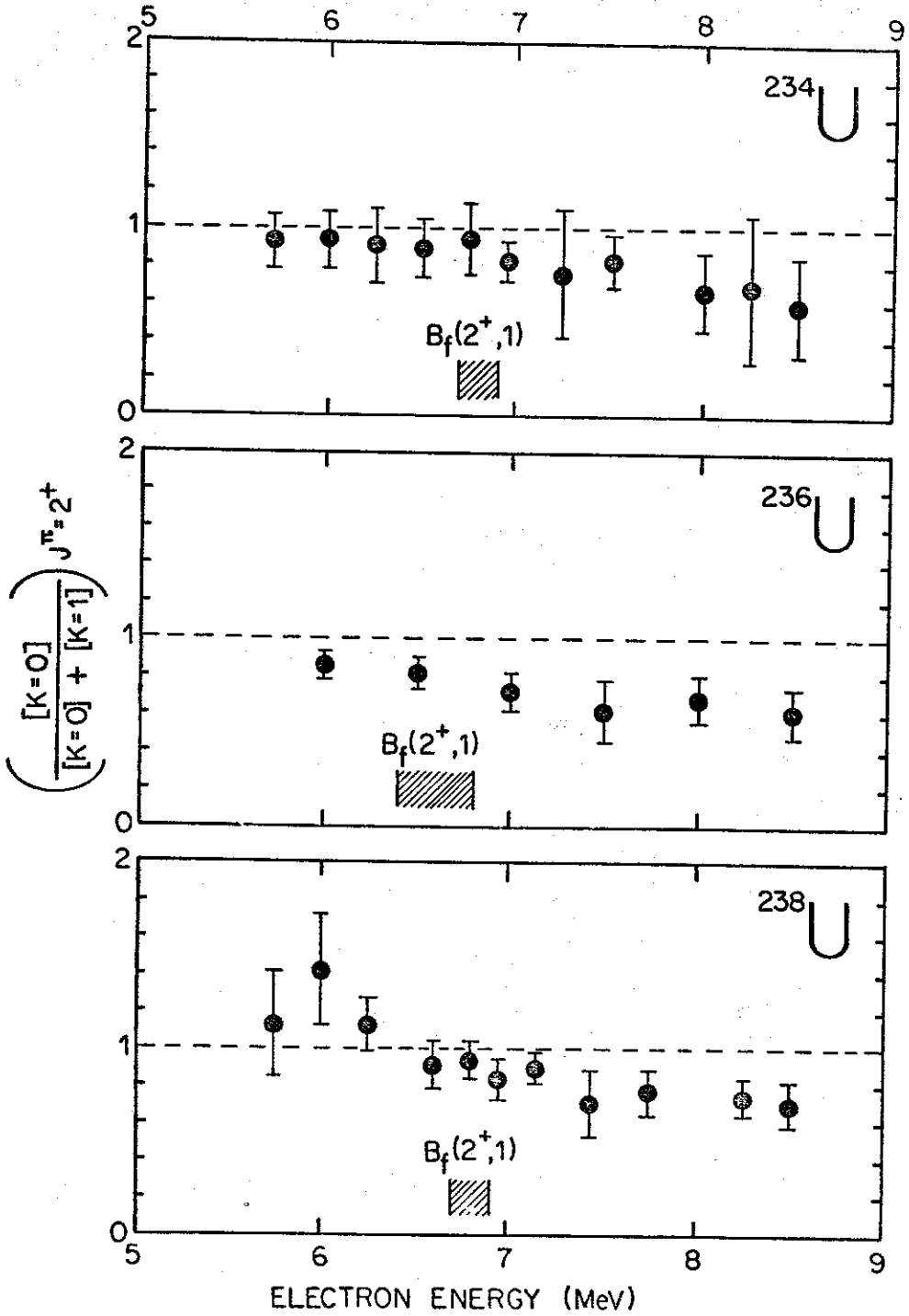
234U
236U
238U
$B_f(2^+,1)$
$\left(\frac{[K=0]}{[K=0]+[K=1]}\right)^{J^\pi=2^+}$
ELECTRON ENERGY (MeV)

Fig. 9